minerals

Article

Petrogenesis and Tectonic Significance of Late Triassic A_1-Type Granite from the West Section of North Qinling Orogenic Belt: Constraints from Geochronology and Geochemistry

Shang Ji [1], Zuochen Li [1,2,*], Xianzhi Pei [1,2,*], Lei Pei [1,2], Ruibao Li [1,2], Chengjun Liu [1,2], Youxin Chen [1,2], Hao Lin [1] and Mao Wang [1]

[1] Key Laboratory of Western China's Mineral Resources and Geological Engineering, Ministry of Education, School of Earth Science and Resources, Chang'an University, Xi'an 710054, China; chdj2022@163.com (S.J.)
[2] Key Laboratory for Mineralization and Efficient Utilization of Critical Metals, Xi'an 710054, China
* Correspondence: lizuochen@chd.edu.cn (Z.L.); peixzh@chd.edu.cn (X.P.)

Abstract: The North China Block and the South China Block collided in the Middle Triassic, but there is still a lack of consensus regarding the end of collisional orogeny and the closure time of the Paleo-Tethys. In this paper, we report zircon U–Pb ages and geochemistry for the Shimen pluton in the northern margin of the West Qinling Orogenic Belt to investigate its genesis and tectonic environment. The new findings allow to constrain the end time of the Triassic orogeny in the Qinling Orogenic Belt and the closure time of the Paleo-Tethys. The weighted average $^{206}Pb/^{238}U$ ages of the Shimen pluton are 218.6 ± 1.5 Ma and 221.0 ± 1.7 Ma. Thus, we suggest that the Shimen pluton crystallized at the 218.6 Ma and 221.0 Ma and was formed during the Late Triassic (Norian). The Shimen pluton is mainly syenogranite and has alkaline dark minerals aegirine–augite. It is composed of 73.45 to 77.80 wt.% SiO_2, 8.28 to 9.76 wt.% alkali, and 11.35 to 13.58 wt.% Al_2O_3, with A/CNK ranging from 0.91 to 1.02 and 10,000 Ga/Al ranging from 2.39 to 3.15. These findings indicate that the Shimen pluton is typical A-type granite. The plutons have low rare earth element contents, ranging from 73.92 to 203.58 ppm, with a moderate negative Eu anomaly. All the samples are enriched in large-ion lithophile elements, such as Rb, Nd, Th and U, and light rare earth elements, and are depleted in high field strength elements, such as Nb, P, Zr, Ba, and Sr. The depletion of Ba, Sr, and Zr may be related to the fractionation and evolution of the granite. According to the petrological and geochemical characteristics, the Shimen pluton is an A_1-type granite formed in an anorogenic extensional environment. Combined with its tectonic characteristics and petrogenesis, the Shimen pluton was probably formed by the partial melting of the crust under high temperature and low pressure in the intraplate environment after the subduction of the South China Block beneath the North China Block. This observation indicates that the Triassic orogeny in the Qinling Orogenic Belt had ended and the Paleo-Tethys-Mianlve Ocean had also closed by the Late Triassic (Norian).

Keywords: zircon U-Pb dating; geochemistry; qinling orogenic belt; petrogenesis; Paleo-Tethys

check for updates

Citation: Ji, S.; Li, Z.; Pei, X.; Pei, L.; Li, R.; Liu, C.; Chen, Y.; Lin, H.; Wang, M. Petrogenesis and Tectonic Significance of Late Triassic A_1-Type Granite from the West Section of North Qinling Orogenic Belt: Constraints from Geochronology and Geochemistry. *Minerals* **2023**, *13*, 557. https://doi.org/10.3390/min13040557

Academic Editor: Manuel Francisco Pereira

Received: 21 February 2023
Revised: 27 March 2023
Accepted: 12 April 2023
Published: 16 April 2023

1. Introduction

The Qinling Orogenic Belt (QOB) is an essential part of the Central China Orogenic Belt [1] (Figure 1a). It is categorized into three blocks: the southern margin of the North China Block, the Qinling Block, and the northern margin of the South China Block, which are bounded by two suture zones: Shangdan Suture Zone (SDSZ) and Mianlve Suture Zone (MLSZ) [1–3]. The North Qinling Belt (NQB) was originally believed to be a part of the North China Block (NCB), but subsequent studies have shown that the Luonan–Luanchuan Fault separates the NQB from the NCB [3–5]. The SDSZ represents the ProtoTethys–Shangdan Ocean suture zone and develops an early Paleozoic magmatic intrusion, while the MLSZ represents the Paleo-Tethys-Mianlve Ocean suture zone and forms an E–W-distributed Triassic granite belt along the suture zone [1,6–12]. The Qinling Mountains are usually divided into the West Qinling and the East Qinling, with the Huicheng Basin as the boundary.

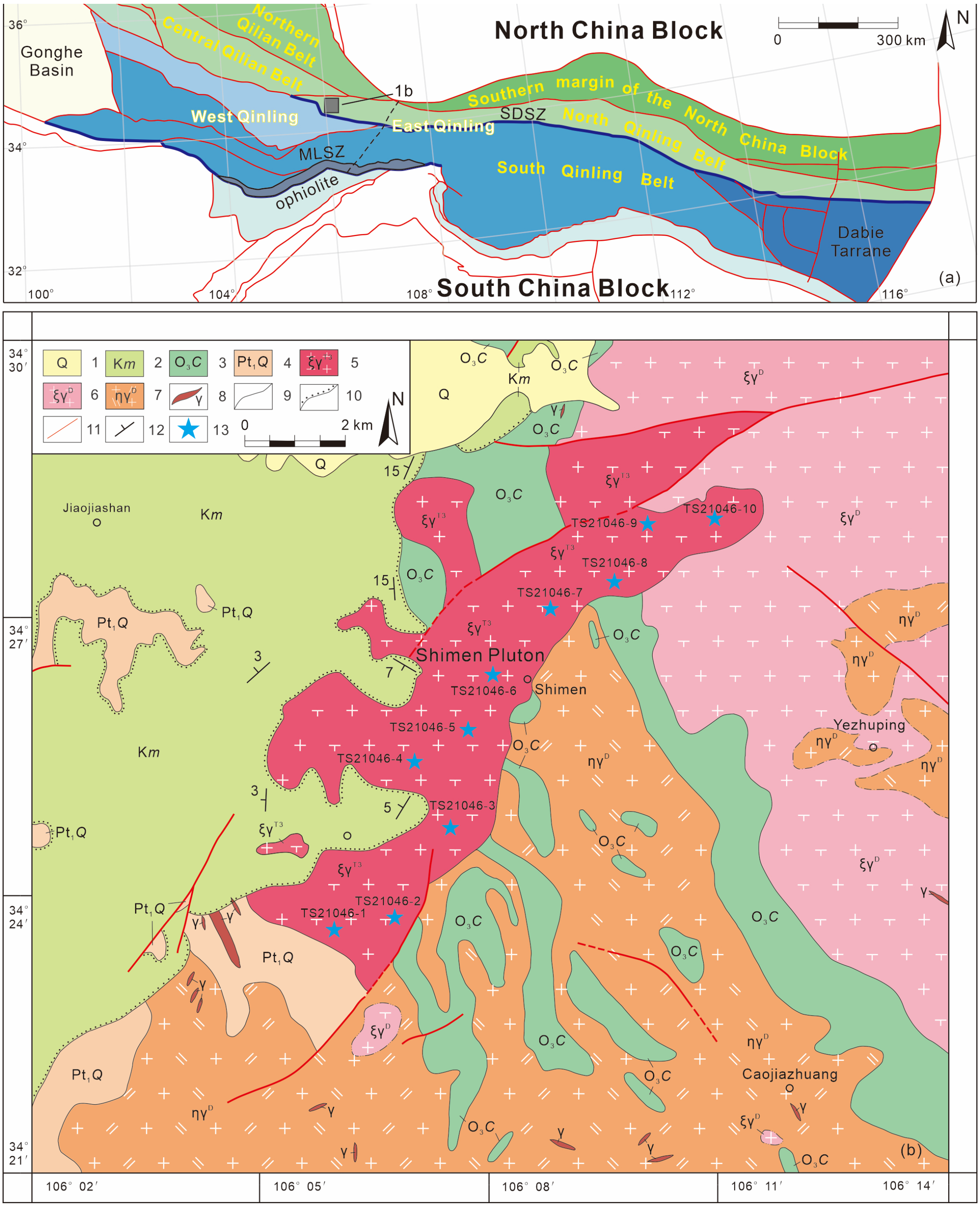

Figure 1. (**a**) Map showing the regional context of the West Qingling Orogenic Belt (WQOB). Geological map modified from Dong et al. [13]. SDSZ = Shangdan Suture Zone; MLSZ = Mianlve Suture Zone; (**b**) Map showing the regional geology of the Shimen pluton in the West Qingling Orogenic Belt. Geological map modified after Pei et al. [14]. 1. Quaternary; 2. Cretaceous Maijishan Formation; 3. Upper Ordovician Caotangou Formation; 4. Lower Proterozoic Qinling Group; 5. Late Triassic Syenogranite; 6. Devonian Syenogranite; 7. Devonian Monzogranite; 8. Granite dikes; 9. Line of Geological limitation; 10. Line of angular unconformity; 11. Fault; 12. Occurrence; 13. Sample location and number.

The QOB has undergone a multiphase and multistage evolutionary process, and finally completed the collision in the Triassic, accompanied by intense magmatic activity [1,6,15–21]. The study of the Triassic pluton in the QOB is of great importance as it elucidates supercontinental events and the evolution of the Paleo-Tethys [13,22–26]. Research shows that numerous magmatic rocks, ophiolites, and metamorphic records are associated with subduction and collision in the MLSZ, which constrained the evolution of the Paleo-Tethys-Mianlve Ocean [12,19,27,28]. Triassic plutons in the study area mainly include (Table 1): (1) Syn-collision environment: Chaijiazhuang pluton [29]; (2) Post-collision environment: Wenquan pluton [30], Shahewan pluton [31], Caoping pluton [31], Zhashui pluton [31], Huangzhuguan pluton [32], Changba pluton [32], and Tianzishan pluton [33]; (3) Post-orogenic environment: Mishuling pluton [26] and Taibai pluton [34]; and (4) Anorogenic environment: Shimen pluton (this paper).

Table 1. Triassic plutons in the study area.

Environment	Pluton	Age (Ma)	Position
Syn-collision	Chaijiazhuang	236.6 ± 2.9	NQB
Post-collision	Tianzishan	241 ± 1.7	NQB
Post-collision	Changba	209.4 ± 0.8~218.3 ± 1.2	SQB
Post-collision	Shahewan	212 ± 0.93	SQB
Post-collision	Wenquan	214 ± 7.1	SQB
Post-collision	Caoping	224.1 ± 1.1	SQB
Post-collision	Zhashui	224.8 ± 1.1	SQB
Post-collision	Huangzhuguan	215.8 ± 0.8~229.2 ± 1.0	SQB
Post-orogenic	Mishuling	214.5 ± 1.6	SQB
Post-orogenic	Taibai	221.8 ± 1.5	SQB
Anorogenic	Shimen	218.6 ± 1.5 and 221.0 ± 1.7	NQB

[SQB] = South Qinling Belt, [NQB] = North Qinling Belt.

The Shimen pluton is located in the Qinling–Qilian Connecting Zone on the northern margin of the West QOB. It was originally classified as a part of the Devonian Dangchuan pluton [35] but was later separated from the Dangchuan pluton; its Rb–Sr isochron age was determined to be 225 Ma [14], and the zircon U-Pb age was 220 ± 2 Ma [36], confirming its formation in the Triassic period.

During the Triassic period, the collision between the NCB and the South China Block (SCB) produced a large number of magmas, which can be categorized into two stages: the early subduction stage (270–235 Ma), and the late collision to the post-collision stage (245–210 Ma) [21,24,25,29,37–43]. The evolution of the crust and the formation of orogenic belts can be investigated by studying and analyzing granites [44–47]. The appearance of A-type granites represents the end of the orogeny, and thus is important for us to understand the end time of the Triassic orogeny in the QOB [48–57]. Therefore, in this paper, we analyzed the zircon U–Pb geochronology and geochemistry of the Shimen pluton in the QOB and discuss the formation age, petrogenesis, and tectonic setting to constrain the end time of the Triassic orogeny in the QOB.

2. Geological Background

The Shimen pluton is located in the Shanggouli–Shimen–Fangmatan area in the north of Dangchuan Township and is distributed in an NNE stripe with an exposed area of about 35,000 km^2 (Figure 1b). The Shimen pluton is located close to the Tianshui–Baoji fault zone, which belongs to the NQB. The Shimen pluton has no evidence of deformation and metamorphism and is clearly distinguishable from its surrounding rocks. In the north, it is in fault contact with the Precambrian granite–gneiss basement Qinling Group [1], and in unconformable contact with the Cretaceous purple conglomerate Maijishan Formation [14]. In the south, it is in intrusive and fault contact with the Late Ordovician low greenschist facies sedimentary and volcanic Caotangou Group [58], and is in contact with a Devonian syenogranite. It should be noted here that the Qinling Group was formed in a post-collision environment or a northward subduction and collision environment of the Shangdan Ocean [8,11,59,60], and the Caotangou Group was formed in an island arc environment [58,61–65].

3. Petrography

The Shimen pluton is a predominantly flesh-red, medium coarse-grained mottled syenogranite with prominent flesh-red field outcrops (Figure 2a,b). It comprises medium-coarse granitic, porphyritic, and massive structures. The syenogranite is composed of orthoclase (40%–45%), plagioclase (20%–25%), quartz (25%–30%), and biotite (3%–5%), with some minor amounts of magnetite, zircon and aegirine–augite (Figure 2c–f). The phenocryst is orthoclase, which is a semi-autogenous columnar, and ranges from 4 mm to 6 mm in size. It occurs as a subhedral columnar texture with cross-hatched twinning, Carlsbad twinning, and is partially kaolinized. In the matrix, orthoclase occurs as a subhedral columnar or allotriomorphic granular texture with Carlsbad twinning and is partially kaolinized, and the crystal size ranges from 0.5 mm to 2 mm. Plagioclase ranges from 0.5 mm to 2.5 mm in size and occurs as grayish white subhedral columnar with polysynthetic twinning and is partially sericitized. Quartz generally measures 0.5 mm to 1.5 mm and occurs as colorless allotriomorphic granules, part of the visible wavy extinction. Biotite is partially altered to chlorite or epidote and occurs as irregular scaly or short columnar, measuring between 0.5 mm and 2.5 mm in size. Aegirine–augite ranges from 0.2 mm to 0.5 mm in size and occurs as yellow-green semi-autogenous columnar shapes.

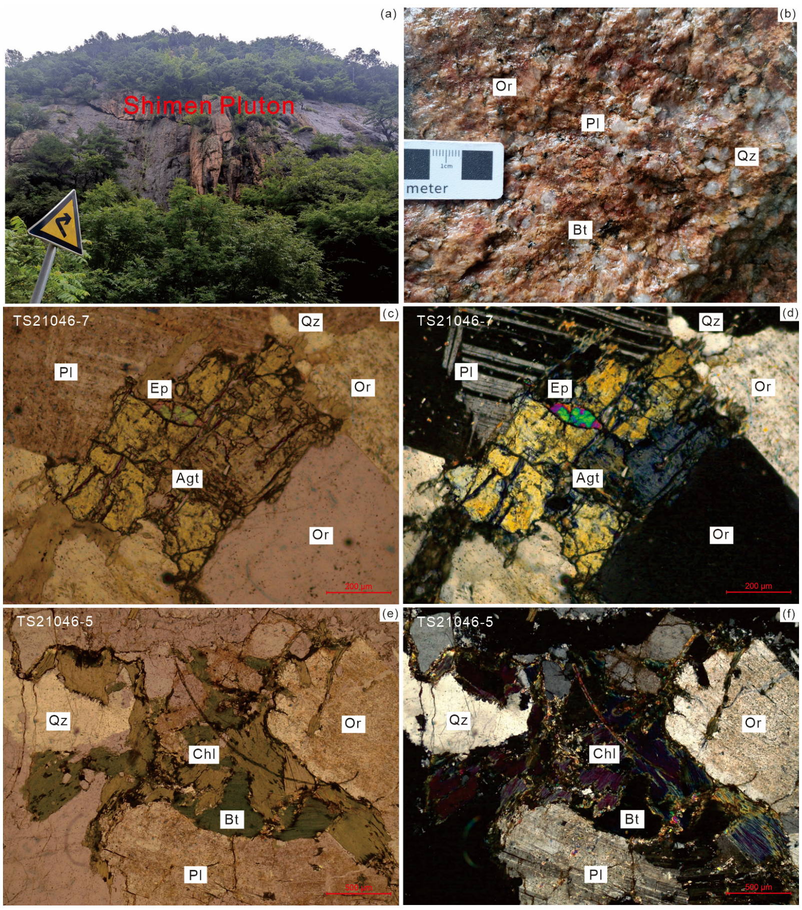

Figure 2. Field photographs and photomicrographs of the Shimen pluton in the WQOB. (**a**,**b**) field photographs of the Shimen pluton; (**c**,**d**) photomicrographs of the Shimen pluton (sample TS21046-7); (**e**,**f**) photomicrographs of the Shimen pluton (sample TS21046-5). Mineral abbreviations are as follows: Pl = plagioclase, Or = orthoclase, Ep = epidote, Agt = aegirine–augite, Qz = quartz, Bt = biotite, Chl = chlorite.

4. Anaytical Methods

4.1. LA-ICP-MS Testing

The zircon U–Pb dating sample was conducted on flesh-red medium coarse–grained mottled syenogranite from the Shimen pluton, and the locations of the two samples are 34°23′38″ N, 106°06′50″ E (TS21046-2) and 34°27′15″ N, 106°08′45″ E (TS21046-7) (Figure 1b).

For the geochronology study, the samples were crushed, and zircon was separated by Xi'an Ruishi Geological Co., Ltd. (Xi'an China). Zircon target fabrication and cathodoluminescence (CL) imaging were completed by Beijing Geoanalysis Ltd. (Beijing, China). Zircon U–Pb isotope was analyzed using laser denudation system NWR193 on PQMS ICP–MS instrument from Jena, Germany. The international-standard zircon 91,500 was used as the standard sample, while the standard zircon GJ-1 was used as the monitoring sample. The data were calculated using the ICPMS Data Cal [66], and the weighted mean age calculation and concordia diagrams were carried out using the Isoplot software package [67]. The detailed analytical method and instrument parameters have already been reported by Li et al. [68].

4.2. Geochemical Analyses

Major, trace, and rare earth elements (REE) were analyzed at the Key Laboratory of Western China's Mineral Resources and Geological Engineering, Ministry of Education, Chang'an University. The major elements were analyzed by X-ray fluorescence spectrometry (XRF). The national standard GB/T14506.28-1993 was used for the XRF tablet dissolution method and has an accuracy better than 2%–3%. The ten samples were baked in an oven at 1000 °C for 90 min and then weighed to obtain the loss on ignition. Trace elements and REEs were measured with Thermo-X7 Inductively Coupled Plasma Mass Spectrometer (ICP-MS).

5. Results of Analyses

5.1. Zircon U-Pb Age

Zircon crystals in the sample (TS21046-2) are predominantly euhedral, with short to long columns. These crystals measure 50 µm to 150 µm in length, and their length to width ratios range from 4:1 to 2:1. The CL images show obvious magmatic oscillatory zoning within the zircon (Figure 3a), indicating a magmatic origin [69–71]. The zircons comprise 183 ppm to 2922 ppm Th and 266 ppm to 4621 ppm U, with the Th/U ratios being 0.35 to 1.14 (Supplementary Table S1). Th and U are positively correlated, and all Th/U ratios are greater than 0.1 (Figure 4a,b), indicating that these zircons are magmatic zircons. The 25 analyses of the sample TS21046-2 show good concordance. A total of 21 concordant analysis points remained after the data with less than 90% concordance were excluded. The weighted average age of $^{206}Pb/^{238}U$ is 221.0 ± 1.7 Ma (MSWD = 0.68, Figure 5a,b).

Zircon crystals in the sample (TS21046-7) are predominantly euhedral, long columnar, and conical. They measured 50 µm to 200 µm in length, with length/width ratios ranging from 5:1 to 1.5:1. The CL images showed obvious magmatic oscillatory zoning within the zircon (Figure 3b), indicating a magmatic origin. The zircons comprise 61 ppm to 2391 ppm Th and 125 ppm to 4485 ppm U, with the Th/U ratios ranging from 0.13 to 1.71 (Supplementary Table S1). Th and U are found to be positively correlated, and the Th/U ratios are all greater than 0.1 (Figure 4c,d). The 25 analyses of the sample TS21046-7 show good concordance. A total of 21 concordant analysis points remained after the data with less than 90% concordance were excluded. The weighted average age of $^{206}Pb/^{238}U$ is 218.6 ± 1.5 Ma (MSWD = 0.39, Figure 5c,d).

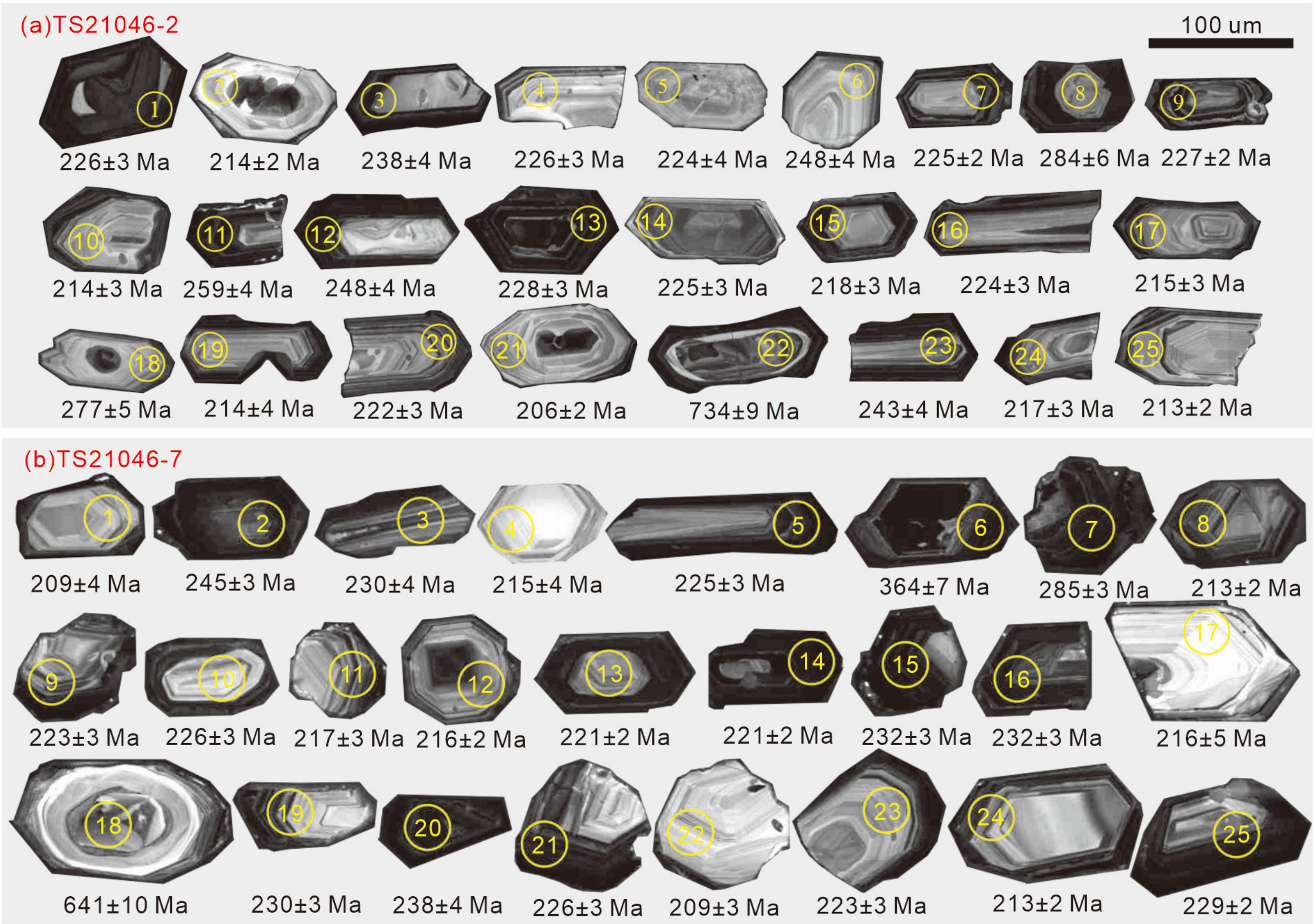

Figure 3. CL images and single-zircon $^{206}Pb/^{238}U$ ages of zircons. (**a**) Sample TS21046-2; (**b**) sample TS21046-7.

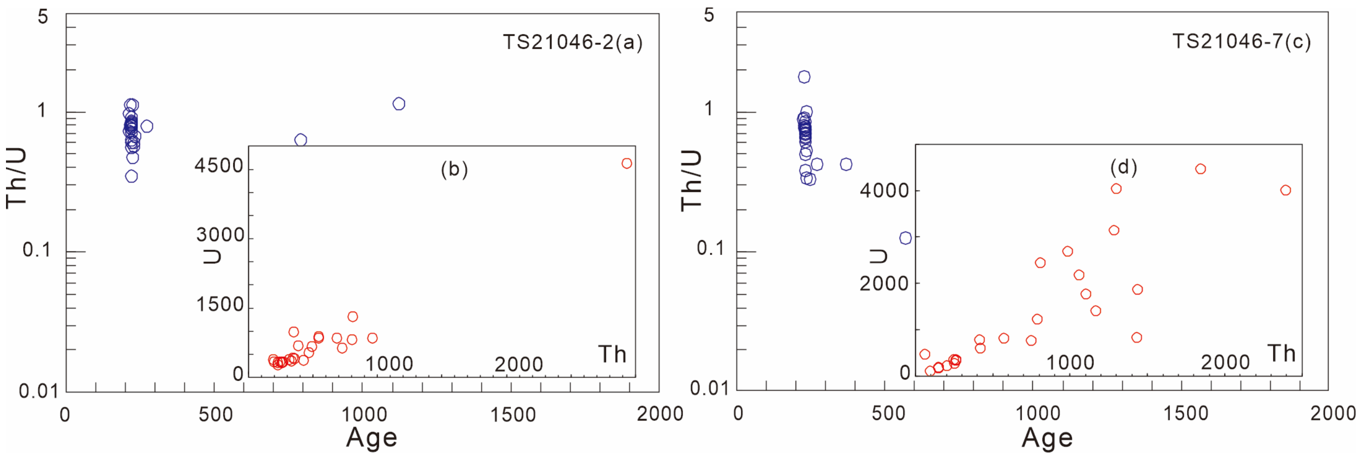

Figure 4. (**a**) Th/U vs. age of zircon diagram of sample TS21046-2; (**b**) Th vs. U content of zircon diagram of sample TS21046-2; (**c**) Th/U vs. age of zircon diagram of sample TS21046-7; (**d**) Th vs. U content of zircon diagram of sample TS21046-7. In subfigure (**a**,**b**), chondrite data for normalization were taken from Sun et al. [72].

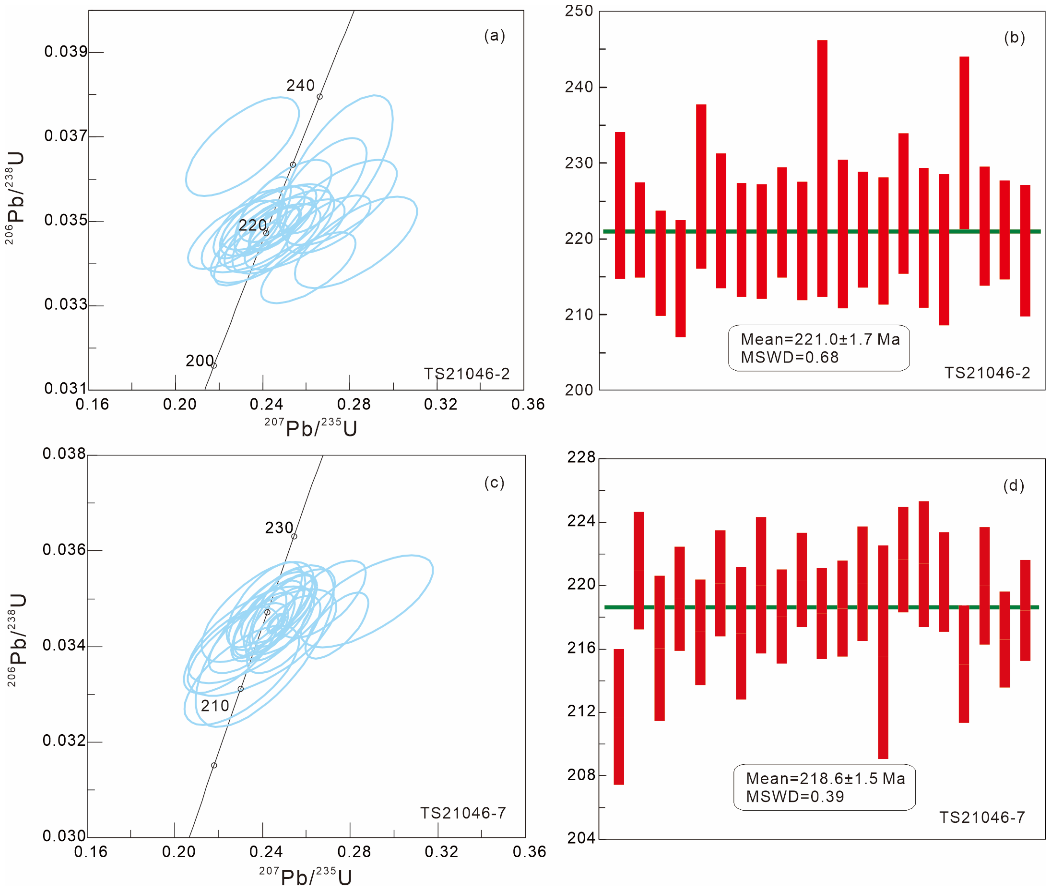

Figure 5. (**a**,**b**) LA-ICP-MS zircon U-Pb concordia diagram of sample TS21046-2; (**c**,**d**) LA-ICP-MS zircon U-Pb concordia diagram of sample TS21046-7 of the Shimen pluton in the WQOB.

5.2. Major and Trace Element Geochemistry

In this paper, all the studied samples have few minerals associated with alteration and metamorphism and have been listed in Supplementary Table S2.

5.2.1. Major Elements

The Shimen pluton has 73.45 to 77.80 wt.% SiO_2, 8.28 to 9.76 wt.% alkali, 11.35 to 13.58 wt.% Al_2O_3, 0.34 to 1.12 wt.% CaO, 0.14 to 0.56 wt.% MgO, 0.09 to 0.39 wt.% TiO_2, and 0.55 to 2.91 wt.% $Fe_2O_3^T$ (Supplementary Table S2). In addition, it has 10,000Ga/Al values between 2.39 to 3.15, and an alkali rate between 4.34 and 5.83. As shown in the total alkali–silica (TAS) diagram (Figure 6a), all the samples are plotted in the granite field and at the boundary between alkaline and subalkaline. As shown in the QAP diagram (Figure 6b), the samples are plotted in the syenogranite field. In the SiO_2–AR diagram (Figure 6c), the samples are plotted in the alkaline field. In the A/NK-A/CNK diagram (Figure 6d), the samples are plotted in the metaluminous field, with A/CNK ranging from 0.91 to 1.02.

5.2.2. Trace Elements

Trace element results indicate that the REE contents of the Shimen pluton range from 73.92 ppm to 203.58 ppm (Supplementary Table S2), ratios of light rare earth element (LREE) to HREE range from 3.92 to 12.64, $(La/Yb)_N$ ratios range from 3.32 to 12.84, and δEu range from 0.39 to 0.92. The chondrite-normalized REE distribution diagram (Figure 7a) for the Shimen pluton shows a right-dipping trend and enrichment in LREE. It also shows a moderate negative Eu anomaly caused by the residual feldspar and garnet in the source region [73].

The primitive mantle-normalized spider diagram (Figure 7b) indicates that the Shimen mottled syenogranite is enriched in large-ion lithophile elements (LILEs), such as Rb, Nd, Th, and U, and depleted in high-field-strength elements (HFSE), such as Nb, P, and Zr, Ba, and Sr. The spider diagram and the REE distribution diagram are almost identical for all samples, indicating their cognate source rocks.

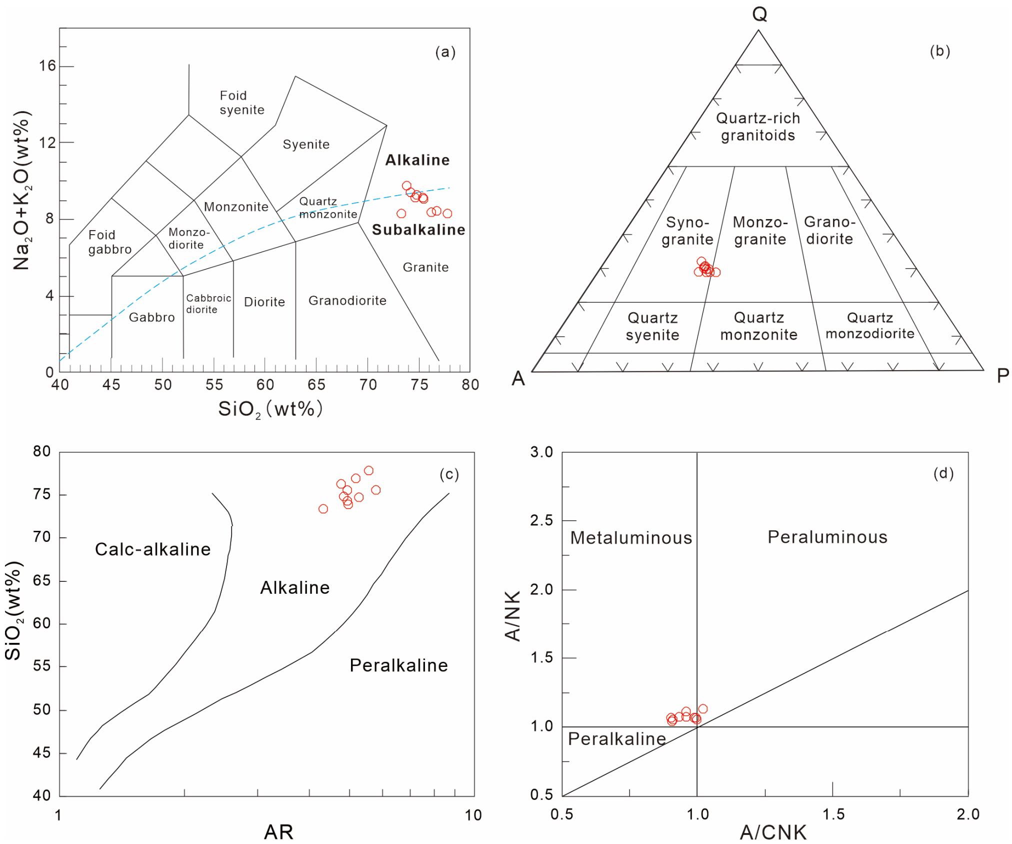

Figure 6. (**a**) TAS diagrams (after Middlemost [74]); (**b**) QAP diagrams (after Streckeisen [75]); (**c**) SiO_2-AR diagrams (after Wright [76]); (**d**) A/NK–A/CNK diagrams (after Maniar and Piccoli [77]) for the Shimen pluton. AR = $(Al_2O_3 + CaO + Na_2O + K_2O)/(Al_2O_3 + CaO - Na_2O - K_2O)$.

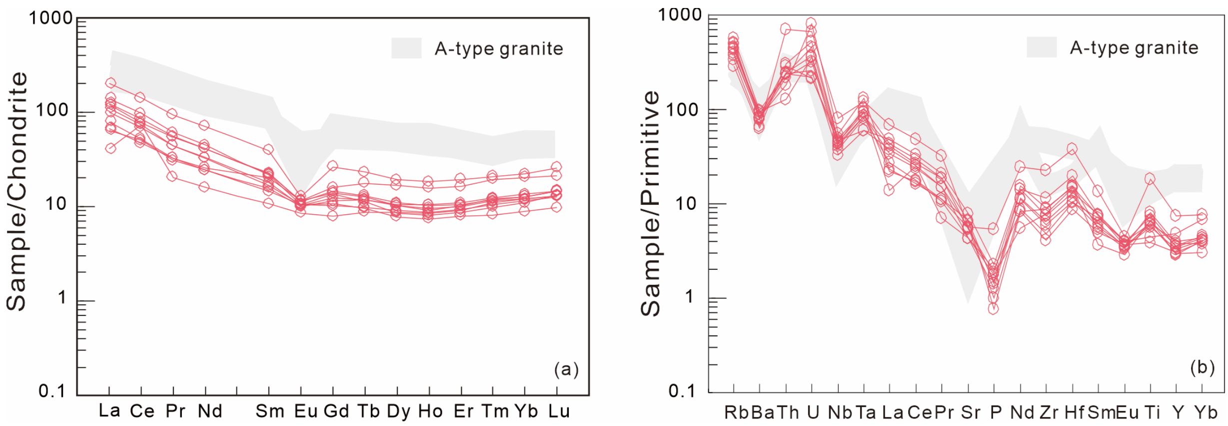

Figure 7. (**a**) Chondrite-normalized rare earth element patterns and (**b**) primitive mantle-normalized trace element spider diagrams for the Shimen pluton in the WQOB (chondrite data and primitive mantle data for normalization were taken from Sun et al. [72]). The data for A-type granitoids are from Collins et al. [49] and Whalen et al. [50].

6. Discussion

6.1. Petrogenesis

A-type granites were originally defined as "alkaline," "anhydrous," and "anorogenic" [48], and later, "aluminous" and "ambiguous" were also added to its definition [56]. A-type granite can be formed in an orogenic environment [50–53,56,57] and can be categorized into two subclasses, A_1 and A_2. The A_1-type granite is mainly formed in an anorogenic environment. In comparison, the A_2-type granite is mainly formed in post-collision and post-orogenic environments [53].

A-type granite is generally characterized by the occurrence of alkaline dark minerals [78–80]. The Shimen pluton is mainly syenogranite and has alkaline dark minerals aegirine–augite. With respect to geochemistry, the Shimen pluton has high SiO_2 and alkali contents and low Al_2O_3 contents, 0.55 to 2.91 $FeO^T/Feo^T + MgO$ values, and 2.39 to 3.15 10,000Ga/Al values. Its chondrite-normalized REE distribution diagram exhibited a right-dip trend with enrichment in LREE and depletion in HREE and a moderate negative Eu anomaly. The primitive mantle-normalized trace element spider diagram indicates that the syenogranite is enriched in LILEs, such as Rb, Nd, Th, and U, and depleted in HFSEs, such as Nb, P, and Zr. All these above are consistent with the characteristics of A-type granites [49,50,52,56,81–85]. In addition, the depletion of Ba, Sr, and Zr may be related to the fractionation and evolution of the granite [86–88].

The syenogranite has high SiO_2 content, but low Zr/Hf values of the whole rock (16.95–22.01), indicating that the Shimen pluton is a highly fractionated granite [89–91]. The compositions of highly fractionated A-type, I-type, and S-type granites showed a strong similarity [54,83,92]. Highly fractionated S-type granites generally have a higher P_2O_5 content (about 0.14%) that decreases with increasing fractionation, while the A-type granites do not show this relationship [54,56]. The P_2O_5 content of the Shimen pluton averages 0.04%, which is much lower than that of highly fractionated S-type granites. In addition, no correlation was observed between content and fractionation, so the Shimen pluton is excluded as an S-type granite. The diagrams presented by Collins [49] and Whalen [50] can be used to distinguish between highly fractionated A-type granite and highly fractionated I-type granite. In the $Na_2O + K_2O$ vs. 10,000Ga/Al diagram, Nb vs. 10,000Ga/Al diagram, MgO/K_2O vs. 10,000Ga/Al diagram, and $(K_2O + Na_2O)/CaO$ vs. 10,000Ga/Al diagram, the samples are located in the field of A-type granite (Figure 8c–f), indicating that the Shimen pluton is an A-type granite.

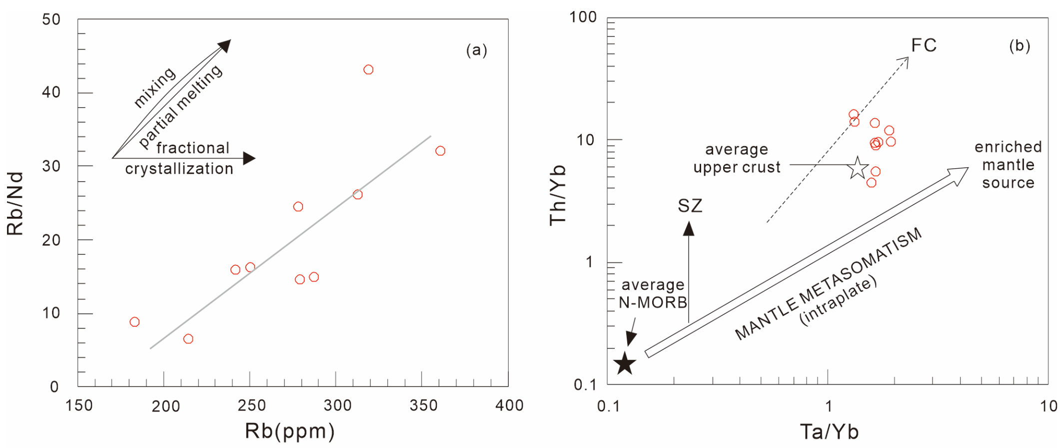

Figure 8. *Cont.*

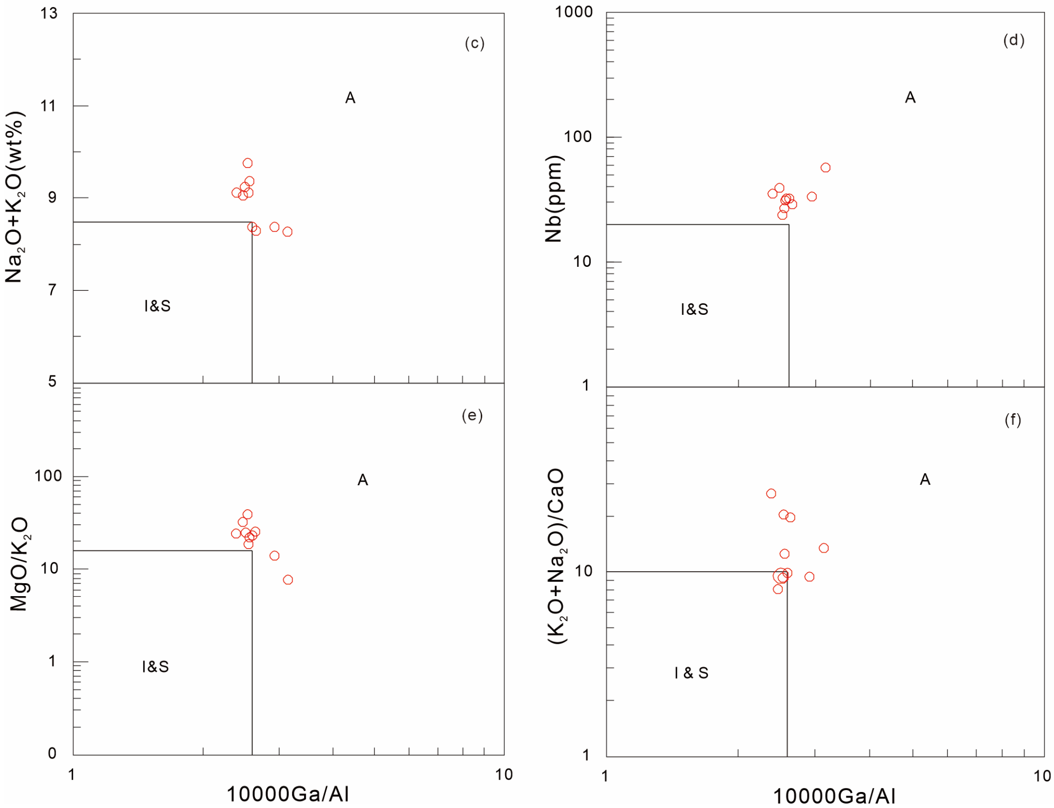

Figure 8. (**a**) Rb/Nd-Rb diagrams (after Schiano et al. [93]); (**b**) Th/Yb vs. Ta/Yb diagrams for the Shimen pluton (after Jahn et al. [94]); (**c**) (Na_2O + K_2O), (**d**)Nb, (**e**)MgO/K_2O and (**f**)((K_2O + Na_2O)/CaO) vs. 10,000Ga/Al discrimination diagrams for the Shimen pluton in the WQOB (after Whalen et al. [50]). A = A-type granitoids; I = I-type granitoids; S = S-type granitoids.

With respect to field geology, the Shimen pluton is NNE-trending, not constrained by the regional tectonic line, and has no obvious deformation and metamorphism [14]. This indicates that the Shimen pluton was formed after the regional tectonic deformation. With respect to geochemistry, the Shimen pluton is a metaluminous alkaline A-type granite, having Y/Nb values between 0.37 to 0.60 and an average of 0.52 (less than 1.2), which corresponds to the characteristics of A-type granite. As shown in the Nb-Y diagram and Ta-Yb diagram (Figure 9a,b), the samples are plotted in the within-plate granites field and the syn-collision granites field. In the Nb-Y-3Ga and Nb-Y-Ce diagrams, all samples are plotted in the A_1-type granite area (Figure 9c,d), indicating that the Shimen pluton is an A_1-type granite and formed in an anorogenic environment.

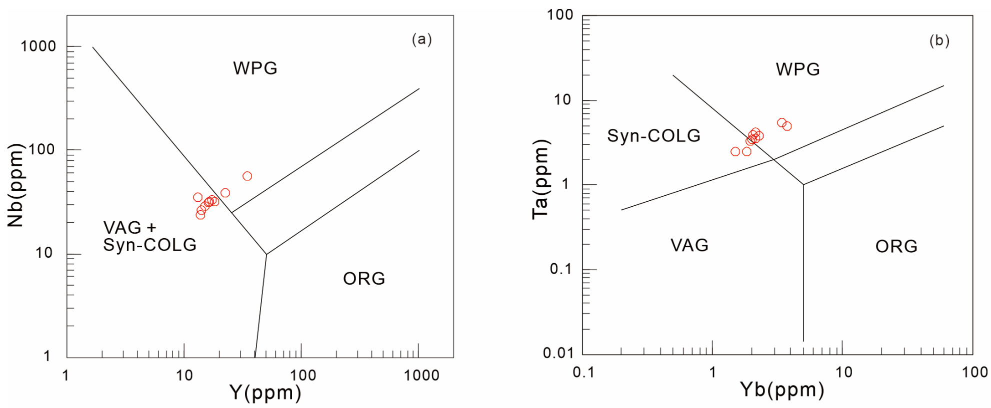

Figure 9. *Cont.*

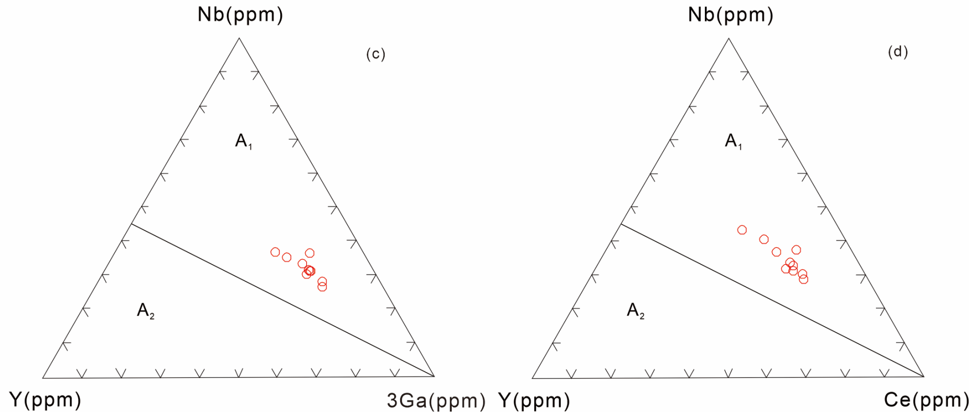

Figure 9. (**a**) Nb-Y diagrams; (**b**) Ta-Yb diagrams for the Shimen Pluton in the WQOB (after Pearce et al. [95]); (**c**) Nb-Y-3Ga diagrams; (**d**) Nb-Y-Ce diagrams for the Shimen Pluton in the WQOB (after Eby [53]). VAG = Volcanic arc granites; Syn-COLG = Syn-collision granites; WPG = Within-plate granites; ORG = Ocean ridge granites. A_1-type = anorogenic environment; A_2-type = post-orogenic environment.

A-type granites are formed in an extensional environment [50,52,77,80,96–99]. Researchers have proposed several views on the formation mechanism of A-type granite: crystallization differentiation of mantle basaltic magma [53,55,100–102], mantle-derived magma mixed with crust-derived magma [102–106], and partial melting of crustal materials [49,54,107,108].

There are no large-scale basaltic rocks and no contemporaneous product of the separation and crystallization of mantle basaltic magma in the vicinity of the Shimen pluton. Therefore, the available geological evidence suggests that the Shimen pluton is not a mantle source. The Shimen pluton is a metaluminous A-type granite (Figure 6d), and the study suggests that the metaluminous A-type granite formed in a high-temperature and low-pressure environment associated with the partial melting of crustal materials [84,98]. The Shimen pluton has 7.61 to 13.64 Nb/Ta values, 1.11 to 3.97 Rb/Sr values, and 16.95 to 22.01 Zr/Hf values. These values are close to the values of crust-derived magma (Nb/Ta value is 11 to 12 in crust-derived magma and 17.5 ± 2 in mantle-derived magma, Rb/Sr value is 3 in crust-derived magma and 15 in mantle-derived magma, Zr/Hf value is 33 in mantle-derived magma) [109–112]. The samples show a partial melting trend in the Rb/Nd–Rb diagram, and on the Th/Yb vs. Ta/Yb diagram, the samples are all located near the crustal field (Figure 8a,b). Previous studies have suggested that the Shimen pluton was formed by the partial melting of crustal materials [36]. In summary, Shimen A-type granite is a crustal source. However, this conclusion is inconsistent with the typical characteristics of A_1-type granite. Therefore, we propose that the Shimen pluton was probably formed by low degree partial melting of crustal materials. Research shows that when the rock is partially melted at a low degree, Nb will be more enriched compared to Y in the molten products [113], so the Y/Nb value will be lower, resulting in the occurrence of A_1-type granite formed by the partial melting of crustal materials, such as China Baicha A_1-type granite [114]. Based on its tectonic characteristics and petrogenesis, it may be the crustal thickening and lithospheric detachment after the subduction between the South China Block and the North China Block, which resulted in the low-level partial melting of crustal materials and the formation of the Shimen A_1-type granite.

6.2. Tectonic Significance

The Qinling Mianlve Ocean existed in the Late Paleozoic to the beginning of the Mesozoic period and was part of the East Paleo-Tethys. It finally closed in the Triassic, accompanied by the collision between the NCB and the SCB, which brought the Chinese mainland into a new evolutionary stage [1,11,12,19,27,28,38,115,116]. The peak time of the collision between the NCB and the SCB was between 235 Ma and 242 Ma, and this collision resulted in the formation of a large number of Mesozoic magmatic rocks [20,38,117,118]. These magmatic rocks were formed between 210 Ma and 242 Ma, with those formed in the syn-collision environment crystallizing at 236 Ma and those formed in the post-collision and post-orogenic environment crystallizing between 210 Ma and 230 Ma [26,30,32,34,38,42,119–123]. The weighted average ages of the Shimen pluton are 218.6 Ma and 221.0 Ma, which is similar to previous research results [14,36], indicating that the Shimen pluton should have been formed in the post-collision and post-orogenic environment. However, the above-mentioned plutons formed in the post-collision and post-orogenic environments are mostly located in the SQB (Table 1) [26,32,38,120], while in the NQB, where the Shimen pluton is located, the Chaijiazhuang pluton crystallized at 236.6 Ma and formed in a syn-collision environment [29], and the Tianzishan pluton crystallized at 241 Ma and formed in a post-collision environment [33], which is not inconsistent with the conclusions reached. The reason for this situation may be that the NQB is located north of the SQB, and the NQB is closer to the collision zone, indicating an earlier occurrence during the collision, so the NQB has probably entered the anorogenic stage and transformed into an intraplate environment, while the SQB is still in the post-collision and post-orogenic stage.

The Triassic orogeny of the QOB has been studied in various aspects. The research on the Early Triassic palaeogeographical characteristics of South Qinling showed that the Early Triassic SQB and the Early Triassic NCB exhibited similar paleolatitude, which is different from that of the Early Triassic SCB. This observation indicates that the SQB was already integrated with the NCB in the Early Triassic, but the SQB and the SCB were still separated by the Paleo-Tethys-Mianlve Ocean [124]. The research on the Triassic granites in the QOB shows that these granites have recorded complete orogenic processes from syn-collision [29], post-collision [30–33], post-orogenic [26,34] to anorogenic environment (this study). The petrogenesis can reflect different tectonic environments and geodynamic backgrounds [46,77,95,125–127]. In this paper, we suggest that the Shimen pluton is A_1-type granite, indicating the continental rifts or intraplate environments [53]. In conclusion, when the Shimen pluton was emplaced (218.6 Ma and 221.0 Ma), the orogeny in this area had already ended, i.e., the Triassic orogeny in the QOB had ended and the Paleo-Tethys-Mianlve Ocean had also closed by the Late Triassic (Norian).

7. Conclusions

From a comprehensive study of the Shimen pluton in the QOB based on geochronology, geochemistry and petrology, we conclude the following.

(1) The LA–ICP–MS zircon ages of the Shimen pluton are 218.6 $\pm$ 1.5 Ma and 221.0 $\pm$ 1.7 Ma, indicating that the intrusion formed in the Late Triassic (Norian).

(2) The Shimen pluton has high SiO_2 and alkali contents and low Al_2O_3 contents. It belongs to metaluminous series and is enriched in LILEs, such as Rb, Nd, Th, and U, and LREE. In addition, it is depleted in HFSE, such as Nb, P, Zr, Ba, and Sr. The Shimen pluton has 10,000Ga/Al values between 2.39 to 3.15, indicating that it is A_1-type granite.

(3) The Shimen pluton is an A_1-type granite formed by the low degree partial melting of the crust in an anorogenic environment. This indicates that the Triassic orogeny in the QOB had ended and the Paleo-Tethys-Mianlve Ocean had also closed by the Late Triassic (Norian).

Supplementary Materials: The following supporting information can be downloaded at: https://www.mdpi.com/article/10.3390/min13040557/s1, Table S1: Zircon LA-ICP-MS U-Pb data of the Shimen pluton in the QOB; Table S2: Whole-rock major and trace element data of the Shimen pluton in the QOB.

Author Contributions: Conceptualization, S.J. and Z.L.; methodology, S.J. and Z.L.; software, L.P., H.L. and M.W.; validation, S.J. and Z.L.; formal analysis, S.J., Z.L., X.P. and R.L.; investigation, S.J., Z.L., H.L., X.P., L.P., C.L. and Y.C.; resources, Z.L. and X.P.; data curation, S.J. and Z.L.; Writing—original draft preparation, S.J. and Z.L.; Writing—review and editing, S.J. and Z.L.; visualization, S.J.; supervi-

sion, Z.L. and X.P.; project administration, Z.L., X.P. and R.L.; funding acquisition, Z.L., X.P. and R.L. All authors have read and agreed to the published version of the manuscript.

Funding: This research was funded by the National Nature Sciences Foundation of China (Grant Nos. 41872235, 42172236, 41802234, 41502191), Natural Science Basic Research Plan in Shaanxi Province of China (Grant Nos. 2019JM-312, 2019JQ-090, 2019JQ-209, 2020JM-229), the Fundamental Research Funds for the Central Universities (Grant Nos. 300102270202, 300103183081, 300103120009, 300104282717, 300102279204, 201810710233), China Scholarship Council (Grant No. 201806565026), and the Youth Innovation Team of Shaanxi Universities.

Data Availability Statement: The original contributions presented in the study are included in the article/Supplementary Material.

Acknowledgments: Thanks are extended to the chief editor and the three anonymous reviewers for their constructive reviews which have greatly improved our manuscript. The authors would like to thank Enago (www.enago.cn (accessed on 20 February 2023)) for the English language review.

Conflicts of Interest: The authors declare no conflict of interest.

References

1. Zhang, G.W.; Zhang, B.R.; Yuan, X.C.; Xiao, Q.H. *Qinling Orogenic Belt and Continental Dynamics*; Science Press: Beijing, China, 2001. (In Chinese with English abstract)
2. Meng, Q.R.; Zhang, G.W. Geologic framework and tectonic evolution of the Qinling orogen, central China. *Tectonophysics* **2000**, *323*, 183–196. [CrossRef]
3. Dong, Y.P.; Zhang, G.W.; Neubauer, F.; Liu, X.M.; Genser, J.; Hauzenberger, C. Tectonic evolution of the Qinling orogen, China: Review and synthesis. *J. Asian Earth Sci.* **2011**, *41*, 213–237. [CrossRef]
4. Zhang, B.R.; Zhang, H.F.; Zhao, Z.D.; Ling, W.L. Geochemical subdivision and evolution of the lithosphere in east Qinling and adjacent regions—Implications for tectonics. *Sci. China Ser. D* **1996**, *39*, 245–255.
5. Dong, Y.P.; Zhang, G.W.; Zhu, B.Q. Tectonic attributes and Proterozoic tectonic evolution of the North Qinling Orogen. *Acta Geosci. Sin.* **2003**, *24*, 3–10. (In Chinese with English abstract)
6. Meng, Q.R.; Zhang, G.W. Timing of collision of the North and South China blocks: Controversy and reconciliation. *Geology* **1999**, *27*, 123–126. [CrossRef]
7. Zhang, G.W.; Dong, Y.P.; Lai, S.C.; Guo, A.L.; Meng, Q.R.; Liu, S.F.; Cheng, S.Y.; Yao, A.P.; Zhang, Z.Q.; Pei, X.Z.; et al. Mianlve structural belt and Mianlve suture zone in the southern margin of Qinling-Dabie Orogenic Belt. *Sci. China Ser. D* **2003**, *33*, 1121–1135. (In Chinese with English abstract)
8. Liu, L.; Liao, X.Y.; Zhang, C.L.; Chen, D.L.; Gong, X.K.; Kang, L. Multi-matemorphic timings of HP-UHP rocks in the North Qinling and their geological implications. *Acta Petrol. Sin.* **2013**, *29*, 1634–1656. (In Chinese with English abstract)
9. Yu, S.; Li, S.Z.; Zhao, S.J.; Cao, H.W.; Suo, Y.H. Long history of a Grenville orogen relic—The North Qinling terrane: Evolution of the Qinling Orogenic Belt from Rodinia to Gondwana. *Precambr. Res.* **2015**, *271*, 98–117. [CrossRef]
10. Zhao, S.J.; Li, S.Z.; Liu, X.; Santosh, M.; Somerville, I.D.; Cao, H.W.; Yu, S.; Zhang, Z.; Guo, L.L. The northern boundary of the Proto-Tethys Ocean: Constraints from structural analysis and U–Pb zircon geochronology of the North Qinling Terrane. *J. Asian Earth Sci.* **2015**, *113*, 560–574. [CrossRef]
11. Dong, Y.P.; Santosh, M. Tectonic architecture and multiple orogeny of the Qinling Orogenic Belt, Central China. *Gondwana Res.* **2016**, *29*, 1–40. [CrossRef]
12. Dong, Y.P.; Sun, S.S.; Santosh, M.; Zhao, J.; Sun, J.P.; He, D.F.; Shi, X.H.; Hui, B.; Cheng, C.; Zhang, G.W. Central China Orogenic Belt and amalgamation of East Asian continents. *Gondwana Res.* **2021**, *100*, 131–194. [CrossRef]
13. Dong, Y.P.; Sun, S.S.; Santosh, M.; Hui, B.; Sun, J.P.; Zhang, F.F.; Cheng, B.; Yang, Z.; Shi, X.H.; He, D.F.; et al. Cross Orogenic Belts in Central China: Implications for the tectonic and paleogeographic evolution of the East Asian continental collage. *Gondwana Res.* **2022**, *109*, 18–88. [CrossRef]
14. Pei, X.Z.; Ding, S.P.; Li, Y.; Su, C.Q.; Li, Y.J.; Chen, S.E.; Yang, J.X.; Zhang, J.; Zhao, X.; Guo, J.F. Regional geological report of the Peoples Republic of China: Tianshui map (I48C002003), scale 1:250,000. Unpublished. 2004; pp. 1–621. (In Chinese with English abstract)
15. Wang, N.W. Micropaleontological study of Lower Palaeozoic siliceous sequences of the Yangtze Platform and Eastern Qinling Range. *J. South Asian Earth Sci.* **1989**, *3*, 141–161.
16. Li, S.G.; Xiao, Y.L.; Liou, D.J.; Chen, Y.Z.; Ge, N.J.; Zhang, Z.Q.; Sun, S.S.; Cong, B.L.; Zhang, R.Y.; Hart, S.R.; et al. Collision of the North China and Yangtse Blocks and formation of coesite-bearing eclogites: Timing and processes. *Chem. Geol.* **1993**, *109*, 89–111. [CrossRef]
17. Zhang, H.F.; Zhang, B.R.; Zhao, Z.D.; Luo, T.C. Crustal subduction and collision in East Qinling Shangdan tectonic belt: Isotopic tracer evidence from granitic magmatic source region. *Sci. China Ser. D* **1996**, *39*, 231–236. (In Chinese with English abstract)
18. Zhai, X.M.; Day, H.W.; Hacker, B.R.; You, Z.D. Paleozoic metamorphism in the Qinling orogen, Tongbai Mountains, central China. *Geology* **1998**, *26*, 371–374. [CrossRef]

19. Pei, X.Z.; Zhang, G.W.; Lai, S.C.; Li, Y.; Chen, L.; Gao, M. Main geological characteristics of Mianlve tectonic belt in the southern margin of West Qinling. *Geol. Bull. China* **2002**, *21*, 486–494. (In Chinese with English abstract)
20. Zheng, Y.F. Research progress of ultrahigh pressure metamorphism and continental collision: A case study of Dabie-Sulu Orogenic Belt. *Chin. Sci. Bull.* **2008**, *53*, 2129–2152. (In Chinese with English abstract)
21. Dong, Y.P.; Zhang, X.N.; Liu, X.M.; Li, W.; Chen, Q.; Zhang, G.W.; Zhang, H.F.; Zhao, Y.; Sun, S.S.; Zhang, F.F. Propagation tectonics and multiple accretionary processes of the Qinling Orogen. *J. Asian Earth Sci.* **2015**, *104*, 84–98. [CrossRef]
22. Zhao, G.C.; Sun, M.; Wilde, S.A.; Li, S.Z. A Paleo-Mesoproterozoic supercontinent: Assembly, growth and breakup. *Earth-Sci. Rev.* **2004**, *67*, 91–123. [CrossRef]
23. Ernst, W.G.; Tsujimori, T.; Zhang, R.; Liou, J.G. Permo-Triassic Collision, Subduction-Zone Metamorphism, and Tectonic Exhumation along the East Asian Continental Margin. *Annu. Rev. Earth Planet. Sci.* **2007**, *35*, 73–110. [CrossRef]
24. Jiang, Y.H.; Jin, G.D.; Liao, S.Y.; Zhou, Q.; Zhao, P. Geochemical and Sr–Nd–Hf isotopic constraints on the origin of Late Triassic granitoids from the Qinling orogen, central China: Implications for a continental arc to continent–continent collision. *Lithos* **2010**, *117*, 183–197. [CrossRef]
25. Chen, Y.J. Indosinian tectonic setting, magmatic activity and mineralization in Qinling Orogenic Belt. *Geol. China* **2010**, *37*, 854–865. (In Chinese with English abstract)
26. Li, Z.C.; Pei, X.Z.; Li, R.B.; Pei, L.; Hu, B.; Liu, C.J.; Chen, G.C.; Chen, Y.X. Geochronology, geochemistry and tectonic setting of the Mishuling pluton in the West Qinling. *Acta Petrol. Sin.* **2013**, *29*, 2617–2634. (In Chinese with English abstract)
27. Zhang, G.W.; Dong, Y.P.; Lai, S.C.; Guo, L.L.; Meng, Q.R.; Liu, F.L.; Cheng, S.Y.; Yao, A.P.; Zhang, Z.Q.; Pei, X.Z.; et al. Mianle tectonic zone and Mianle suture zone on southern margin of Qinling-Dabie Orogenic Belt. *Sci. China Earth Sci.* **2004**, *47*, 300–316. [CrossRef]
28. Dong, Y.P.; Zhang, G.W.; Hauzenberger, C.; Neubauer, F.; Yang, Z.; Liu, X.M. Palaeozoic tectonics and evolutionary history of the Qinling orogen: Evidence from geochemistry and geochronology of ophiolite and related volcanic rocks. *Lithos* **2011**, *122*, 39–56. [CrossRef]
29. Li, X.F.; Li, Y.S.; Dong, G.C.; Lv, X.; Xia, Q. Indosinian granitic magmatism and tectonic evolution in the eastern part of the West Qinling: Geochemistry, zircon U-Pb chronology, and Hf isotope constraints. *Acta Petrol. Sin.* **2021**, *37*, 1691–1712. (In Chinese with English abstract)
30. Zhu, L.M.; Ding, Z.J.; Yao, S.Z.; Zhang, G.W.; Song, S.G.; Qu, W.J.; Guo, B.; Li, B. Metallogenic geological events and metallogenic tectonic setting of Wenquan Molybdenum deposit in the West Qinling, Gansu Province. *Chin. Sci. Bull.* **2009**, *54*, 2337–2347 + 2439–2441. (In Chinese with English abstract) [CrossRef]
31. Gong, H.J.; Zhu, L.M.; Sun, B.Y.; Li, B.; Guo, B. Zircon U-Pb ages, Hf isotope characteristics and geological setting of Shahewan, Caoping and Zhashui plutons in the South Qinling. *Acta Petrol. Sin.* **2009**, *25*, 248–264. (In Chinese with English abstract)
32. Wei, R.; Wang, Y.T.; Hu, Q.Q.; Huang, S.K.; Yuan, Q.H.; Bai, Q.L.; Hu, W.R.; Zhang, X.J.; Cai, T. Zircon U-Pb ages, Hf isotopic compositions and geological setting of Changba and Huangzhuguan plutons in the West Qinling. *Miner. Deposits.* **2017**, *36*, 1367–1386. (In Chinese with English abstract)
33. Lv, Y.B. Characteristics and Petrogenesis of Tianzishan Pluton in Liziyuan-Taiyangsi Ore Concentration Area, Gansu Province. Master's Thesis, China University of Geosciences, Beijing, China, 2019. (In Chinese with English abstract)
34. Ren, H.Z.; Pei, X.Z.; Liu, C.J.; Li, Z.C.; Li, R.B.; Wei, B.; Chen, W.N.; Wang, Y.Y.; Xu, X.C.; Liu, T.J.; et al. LA-ICP-MS Zircon U-Pb Age, geochemistry and geological setting of Taibai pluton in Tianshui area, West Qinling. *Geol. Bull. China* **2014**, *33*, 1041–1054. (In Chinese with English abstract)
35. Regional Geological Survey Team of Shaanxi Provincial Geological Bureau. Regional Geological Report of the Peoples Republic of China: Tianshui Map, Scale 1:200,000. Unpublished. 1968. (In Chinese with English abstract)
36. Wang, J.; Zhang, H.F.; Xu, W.C.; Cai, H.M. The genesis and tectonic significance of granites in the Dangchuan area of the West Qinling. *Earth Sci. J. China Univ. Geosci.* **2008**, *33*, 474–486. (In Chinese with English abstract)
37. Yin, A.; Nie, S.Y. An indentation model for the North and South China collision and the development of the Tan-Lu and Honam Fault Systems, eastern Asia. *Tectonics* **1993**, *12*, 801–813. [CrossRef]
38. Li, S.G.; Sun, W.D.; Zhang, G.W.; Chen, J.Y.; Yang, Y.C. Chronology and geochemistry of the Heigouxia metamorphic volcanic rocks in Mian-lue Suture zone, South Qinling: Evidence of Paleozoic Ocean basin and its closing age. *Sci. China Ser. D* **1996**, *33*, 300–310.
39. Lu, X.X.; Dong, Y.; Chang, Q.L.; Xiao, Q.H.; Li, X.B.; Wang, X.X. Indosinian Shahewan rapakivi granite in Qinling and its dynamic significance. *Sci. China Ser. D* **1996**, *33*, 266–272.
40. Wang, X.X.; Wang, T.; Jahn, B.M.; Hu, N.G.; Chen, W. Tectonic significance of Late Triassic post-collisional lamprophyre dykes from the Qinling Mountains (China). *Geol. Mag.* **2007**, *144*, 837–848. [CrossRef]
41. Yang, P.T.; Liu, S.W.; Li, Q.G.; Wang, Z.Q.; Wang, R.T.; Wang, W. Geochemistry and zircon U-Pb-Hf isotopic systematics of the Ningshan granitoid batholith, middle segment of the south Qinling belt, Central China: Constraints on petrogenesis and geodynamic processes. *J. Asian Earth Sci.* **2012**, *61*, 166–186. [CrossRef]
42. Wang, X.X.; Wang, T.; Zhang, C.L. Neoproterozoic, Paleozoic, and Mesozoic granitoid magmatism in the Qinling Orogen, China: Constraints on orogenic process. *J. Asian Earth Sci.* **2013**, *72*, 129–151. [CrossRef]
43. Chen, Y.J.; Santosh, M. Triassic tectonics and mineral systems in the Qinling Orogen, central China. *Geol. J.* **2014**, *49*, 338–358. [CrossRef]

44. Wang, D.Z.; Shu, L.S. Granite tectonic magmatic association. *Geol. China* **2007**, *13*, 362–370.
45. Brown, M. Granite: From genesis to emplacement. *Geol. Soc. Am. Bull.* **2012**, *125*, 1079–1113. [CrossRef]
46. Clemens, J.D.; Stevens, G. What controls chemical variation in granitic magmas. *Lithos* **2012**, *134*, 317–329. [CrossRef]
47. Xu, X.S.; He, Z.Y. Progress in granite research. *Bull. Mineral. Petrol. Geochem.* **2012**, *31*, 205–209.
48. Loiselle, M.C.; Wones, D.R. Characteristics and origin of anorogenic granites. *Geol. Soc. Am. Abstr. Prog.* **1979**, *11*, 468.
49. Collins, W.J.; Beams, S.; White, A.J.R.; Chappell, B.W. Nature and origin of A-type granites with particular reference to southeastern Australia. *Contrib. Mineral. Petrol.* **1982**, *80*, 189–200. [CrossRef]
50. Whalen, J.B.; Currie, K.L.; Chappell, B.W. A-type granites: Geochemical characteristics, discrimination and petrogenesis. *Contrib. Mineral. Petrol.* **1987**, *95*, 407–419. [CrossRef]
51. Bonin, B. From orogenic to anorogenic settings: Evolution of granitoid suites after a major orogenesis. *Geol. J.* **1990**, *25*, 261–270. [CrossRef]
52. Eby, G.N. The A-type granitoids: A review of their occurrence and chemical characteristics and speculations on their petrogenesis. *Lithos* **1990**, *26*, 115–134. [CrossRef]
53. Eby, G.N. Chemical subdivision of the A-type granitoids: Petrogenetic and tectonic implications. *Geology* **1992**, *20*, 641–644. [CrossRef]
54. King, P.L.; White, A.J.R.; Chappell, B.W.; Allen, C.M. Characterization and Origin of Aluminous A-type Granites from the Lachlan Fold Belt, Southeastern Australia. *J. Petrol.* **1997**, *38*, 371–391. [CrossRef]
55. Mushkin, A.; Navon, O.; Halicz, L.; Hartmann, G.; Stein, M. The Petrogenesis of A-type Magmas from the Amram Massif, Southern Israel. *J. Petrol.* **2003**, *44*, 815–832. [CrossRef]
56. Bonin, B. A-type granites and related rocks: Evolution of a concept, problems and prospects. *Lithos* **2007**, *97*, 1–29. [CrossRef]
57. Xiao, E.; Qiu, J.S.; Xu, X.S.; Jiang, S.Y.; Hu, J.; Li, Z. Chronology, geochemistry, petrogenesis and tectonic implications of Yaokeng Alkaline granites in Zhejiang Province. *Acta Petrol. Sin.* **2007**, *23*, 1431–1440. (In Chinese with English abstract)
58. Xu, X.C.; Pei, X.Z.; Liu, C.J.; Li, R.B.; Li, Z.C.; Wei, B.; Wang, Y.Y.; Liu, T.J.; Ren, H.Z. Geochemical characteristics and geological setting of Early Paleozoic volcanic rocks in Yinyagou Group, Tianshui area, West Qinling. *Geol. China* **2014**, *41*, 851–865. (In Chinese with English abstract)
59. Wu, Y.B.; Zheng, Y.F. Tectonic evolution of a composite collision orogen: An overview on the Qinling–Tongbai–Hong'an–Dabie–Sulu Orogenic Belt in central China. *Gondwana Res.* **2013**, *23*, 1402–1428. [CrossRef]
60. Liu, P.L.; Wu, Y.; Liu, Q.H.; Zhang, J.F.; Zhang, L.; Jin, Z.M. Partial melting of UHP calc-gneiss from the Dabie Mountains. *Lithos* **2014**, *192*, 86–101. [CrossRef]
61. Hu, B. Geochemical Characteristics and Tectonic Setting of Early Paleozoic Metamorphic Volcanic Rocks in Qingshui-Zhangjiachuan, Tianshui Area, Gansu Province. Master's Thesis, Chang'an University, Xi'an, China, 2005. (In Chinese with English abstract)
62. He, S.P.; Wang, H.L.; Xu, X.Y.; Zhang, H.F.; Ren, G.M. Geochemical characteristics and tectonic environment of Hongtubao basic volcanic rocks and Chenjiahe medium-acid volcanic rocks in the eastern part of North Qilian belt. *Acta Petrol. Mineral.* **2007**, *26*, 295–309.
63. Wang, Y. Petrological Characteristics and Tectonic Setting of the Hongtubao Metamorphic Basic Volcanic Rocks in the Huluhe Group, Tianshui Area, Gansu Province. Master's Thesis, Chang'an University, Xi'an, China, 2011.
64. Wang, D.Y. Volcanic rock correlation and tectonic environment analysis of Caotangou group and Danfeng group. *Northwest. Geol.* **2002**, *35*, 59–66. (In Chinese with English abstract)
65. Yan, Q.R.; Wang, Z.Q.; Chen, J.L.; Yan, Z.; Wang, T.; Li, Q.G.; Jiang, C.F.; Zhang, Z.Q. Geochemical and isotopic constraints, SHRIMP ages and implications of volcanic rocks in the Qiyuguan Group and Caotangou Group, North Qinling belt. *Acta Geol. Sin.* **2007**, *81*, 488–500. (In Chinese with English abstract)
66. Liu, Y.S.; Hu, Z.C.; Zong, K.Q.; Gao, C.G.; Gao, S.; Xu, J.; Chen, H.H. Reappraisement and refinement of zircon U-Pb isotope and trace element analyses by LA-ICP-MS. *Chin. Sci. Bull.* **2010**, *55*, 1535–1546. [CrossRef]
67. Ludwig, K.R. User's Manual for Isoplot 3.00-A Geochronological Toolkit for Microsoft Excel. *Berkeley Geochronl. Cent. Spec. Publ.* **2003**, *4*, 25–32.
68. Li, H.K.; Geng, J.Z.; Hao, S.; Zhang, Y.Q.; Li, H.M. Determination of zircon U-Pb isotope ages by laser Ablation multi-receiver Plasma Mass Spectrometer (LA-MC-ICPMS). *Acta Mineral. Sin.* **2009**, *29*, 600–601. (In Chinese with English abstract)
69. Belousova, E.A.; Griffin, W.L.; O'reilly, S.Y.; Fisher, N.I. Igneous zircon: Trace element composition as an indicator of source rock type. *Contrib. Mineral. Petrol.* **2002**, *143*, 602–622. [CrossRef]
70. Wu, Y.B.; Zheng, Y.F. Genesis of zircon and its constraints on interpretation of U-Pb age. *Chin. Sci. Bull.* **2004**, *49*, 1554–1569. [CrossRef]
71. Siebel, W.; Blaha, U.; Chen, F.; Rohrmüller, J. Geochronology and geochemistry of a dyke–host rock association and implications for the formation of the Bavarian Pfahl shear zone, Bohemian Massif. *Int. Earth Sci.* **2005**, *94*, 8–23. [CrossRef]
72. Sun, S.S.; Mcdonough, W.F. Chemical and isotopic systematics of oceanic basalts: Implications for mantle composition and processes. *Geol. Soc. Lond. Spec. Publ.* **1989**, *42*, 313–345. [CrossRef]
73. Patiño Douce, A.E.; Johnston, A.D. Phase equilibria and melt productivity in the pelitic system: Implications for the origin of peraluminous granitoids and aluminous granulites. *Contrib. Mineral. Petrol.* **1991**, *107*, 202–218. [CrossRef]
74. Middlemost, E.A.K. Naming materials in the magma/igneous rock system. *Earth-Sci. Rev.* **1994**, *37*, 215–224. [CrossRef]

75. Streckeisen, A. Plutonic rock: Classification and nomenclature recommended by the IUGS Subcommission on the Systematics of Igneous Rocks. *Geotimes* **1973**, *18*, 26–30. [CrossRef]
76. Wright, J.B. A simple alkalinity ratio and its application to questions of non-orogenic granite genesis. *Geol. Mag.* **1969**, *106*, 370–384. [CrossRef]
77. Maniar, P.D.; Piccoli, P.M. Tectonic discrimination of granitoids. *Geol. Soc. Am. Bull.* **1989**, *101*, 635–643. [CrossRef]
78. Eby, G.N.; Woolley, A.R.; Din, V.K.; Platt, G. Geochemistry and Petrogenesis of Nepheline Syenites: Kasungu–Chipala, Ilomba, and Ulindi Nepheline Syenite Intrusions, North Nyasa Alkaline Province, Malawi. *J. Petrol.* **1998**, *39*, 1405–1424. [CrossRef]
79. Wei, D.L.; Xia, B.; Zhang, Y.Q.; Wang, R.; Wan, S.K. Pyroxene composition and petrochemical characteristics of Zhuopan-Liuhe alkaline rocks in west Yunnan Province. *Mineral. Petrol.* **2005**, *25*, 15–19. (In Chinese with English abstract)
80. Jia, X.H.; Wang, Q.; Tang, G.J. Research progress and significance of A-type granites. *Geotecton. Metallog.* **2009**, *33*, 465–480. (In Chinese with English abstract)
81. Landenberger, B.; Collins, W.J. Derivation of A-type Granites from a Dehydrated Charnockitic Lower Crust: Evidence from the Chaelundi Complex, Eastern Australia. *J. Petrol.* **1996**, *37*, 145–170. [CrossRef]
82. Chen, P.R.; Zhang, B.T.; Kong, X.G.; Cai, B.C.; Ling, H.F.; Ni, Q.S. Geochemical characteristics and tectonic geological setting of Zhaibei A-type granite in south Jiangxi Province. *Acta Petrol. Sin.* **1998**, *14*, 22–31. (In Chinese with English abstract)
83. Wu, F.Y.; Li, X.H.; Yang, J.H.; Zheng, Y.F. Some problems in the study of granite petrogenesis. *Acta Petrol. Sin.* **2007**, *23*, 1217–1238. (In Chinese with English abstract)
84. Frost, C.D.; Frost, B.R. On Ferroan (A-type) Granitoids: Their Compositional Variability and Modes of Origin. *J. Petrol.* **2011**, *52*, 39–53. [CrossRef]
85. Zhang, Q.; Ran, H.; Li, C.D. What is the essence of A-type granite? *Acta Petrol. Mineral.* **2012**, *31*, 621–626. (In Chinese with English abstract)
86. Gelman, S.E.; Deering, C.D.; Bachmann, O.; Huber, C.; Gutiérrez, F. Identifying the crystal graveyards remaining after large silicic eruptions. *Earth Planet. Sci. Lett.* **2014**, *403*, 299–306. [CrossRef]
87. Lee, C.T.A.; Morton, D.M. High silica granites: Terminal porosity and crystal settling in shallow magma chambers. *Earth Planet. Sci. Lett.* **2015**, *409*, 23–31. [CrossRef]
88. Wu, F.Y.; Liu, X.C.; Ji, W.Q.; Wang, J.M.; Yang, L. Identification and research of highly fractionated granite. *Sci. China* **2017**, *47*, 745–765. (In Chinese with English abstract)
89. Bau, M. Controls on the fractionation of isovalent trace elements in magmatic and aqueous systems: Evidence from Y/Ho, Zr/Hf, and lanthanide tetrad effect. *Contrib. Mineral. Petrol.* **1996**, *123*, 323–333. [CrossRef]
90. Breiter, K.; Lamarão, C.N.; Borges, R.M.K.; Dall'agnol, R. Chemical characteristics of zircon from A-type granites and comparison to zircon of S-type granites. *Lithos* **2014**, *192*, 208–225. [CrossRef]
91. Deering, C.D.; Keller, B.; Schoene, B.; Bachmann, O.; Beane, R.J.; Ovtcharova, M. Zircon record of the plutonic-volcanic connection and protracted rhyolite melt evolution. *Geology* **2016**, *44*, 267–270. [CrossRef]
92. Gao, P.; Zheng, Y.F.; Zhao, Z.F. Distinction between S-type and peraluminous I-type granites: Zircon versus whole-rock geochemistry. *Lithos* **2016**, *258*, 77–91. [CrossRef]
93. Schiano, P.; Monzier, M.; Eissen, J.P.; Martin, H.; Koga, K.T. Simple mixing as the major control of the evolution of volcanic suites in the Ecuadorian Andes. *Contrib. Mineral. Petrol.* **2010**, *160*, 297–312. [CrossRef]
94. Jahn, B.M.; Wu, F.; Lo, C.H. Crust-mantle Interaction Induced by Deep Subduction of the Continental Crust: Geochemical and Sr-Nd Isotopic Evidence from Post-collisional Mafic-ultramafic Intrusions of the Northern Dabie Complex, Central China. *Chem. Geol.* **1999**, *157*, 119–146. [CrossRef]
95. Pearce, J.A.; Harris, N.; Tindle, A.G. Trace Element Discrimination Diagrams for the Tectonic Interpretation of Granitic Rocks. *J. Petrol.* **1984**, *25*, 956–983. [CrossRef]
96. Clemens, J.D.; Holloway, J.R.; White, A.J.R. Origin of an A-type granite; experimental constraints. *Am. Mineral.* **1986**, *71*, 317–324.
97. Hong, D.W.; Wang, S.G.; Han, B.F.; Jin, M.Y. Tectonic environment classification and identification of alkaline granite. *Sci. China Ser. B* **1995**, *25*, 418–426. (In Chinese with English abstract)
98. Douce, A.E.P. Generation of metaluminous A-type granites by low-pressure melting of calc-alkaline granitoids. *Geology* **1997**, *25*, 743–746. [CrossRef]
99. Dall'agnol, R.; Frost, C.D.; Rämö, O.T. A-Type Granites and Related Rocks Through Time. *Geochim. Cosmochim. Acta* **2005**, *69*, A79.
100. Litvinovsky, B.A.; Jahn, B.M.; Zanvilevich, A.N.; Saunders, A.D.; Poulain, S.; Kuzmin, D.V.; Reichow, M.; Titov, A.V. Petrogenesis of syenite-granite suites from the Bryansky Complex (Transbaikalia, Russia): Implications for the origin of A-type granitoid magmas. *Chem. Geol.* **2002**, *189*, 105–133. [CrossRef]
101. Anderson, I.C.; Frost, C.D.; Frost, B.R. Petrogenesis of the Red Mountain pluton, Laramie anorthosite complex, Wyoming: Implications for the origin of A-type granite. *Precambr. Res.* **2003**, *124*, 243–267. [CrossRef]
102. Weissman, A.; Kessel, R.; Navon, O.; Stein, M. The petrogenesis of calc-alkaline granites from the Elat massif, Northern Arabian-Nubian shield. *Precambr. Res.* **2013**, *236*, 252–264. [CrossRef]
103. Goodenough, K.M.; Upton, B.J.G.; Ellam, R.M. Geochemical evolution of the Ivigtut granite, South Greenland: A fluorine-rich "A-type" intrusion. *Lithos* **2000**, *51*, 205–221. [CrossRef]
104. Kemp, A.I.S.; Wormald, R.; Whitehouse, M.J.; Price, R.C. Hf isotopes in zircon reveal contrasting sources and crystallization histories for alkaline to peralkaline granites of Temora, southeastern Australia. *Geology* **2005**, *33*, 797–800. [CrossRef]

105. Yang, J.H.; Wu, F.Y.; Chung, S.L.; Wilde, S.A.; Chu, M.F. A hybrid origin for the Qianshan A-type granite, northeast China: Geochemical and Sr–Nd–Hf isotopic evidence. *Lithos* **2006**, *89*, 89–106. [CrossRef]
106. Ma, C.Q.; Xiong, F.H.; Yin, S.; Wang, L.X.; Gao, K. The intensity and cycle of magmatism in the Orogenic Belt: A case study of the Paleo-Tethys granitoids in East Kunlun belt. *Acta Petrol. Sin.* **2015**, *31*, 3555–3568. (In Chinese with English abstract)
107. Droop, G.T.R.; Clemens, J.D.; Dalrymple, D. Processes and Conditions during Contact Anatexis, Melt Escape and Restite Formation: The Huntly Gabbro Complex, NE Scotland. *J. Petrol.* **2003**, *44*, 995–1029. [CrossRef]
108. Yang, S.Y.; Jiang, S.Y.; Zhao, K.D.; Jiang, Y.H.; Ling, H.F.; Luo, L. Geochronology, geochemistry and tectonic significance of two Early Cretaceous A-type granites in the Gan-Hang Belt, Southeast China. *Lithos* **2012**, *150*, 155–170. [CrossRef]
109. Green, T.H. Significance of Nb/Ta as an indicator of geochemical processes in the crust-mantle system. *Chem. Geol.* **1995**, *120*, 347–359. [CrossRef]
110. Bea, F.; Arzamastsev, A.A.; Montero, P.; Arzamastseva, L.V. Anomalous alkaline rocks of Soustov, Kola: Evidence of mantle-derived metasomatic fluids affecting crustal materials. *Contrib. Mineral. Petrol.* **2001**, *140*, 554–566. [CrossRef]
111. Rudnick, R.L. 3.01—Composition of the Continental Crust. *Treatise Geochem.* **2003**, *3*, 1–64.
112. Gao, S.; Rudnick, R.L.; Yuan, H.L.; Liu, X.M.; Liu, Y.S.; Xu, W.L.; Ling, W.L.; Ayers, J.C.; Wang, X.; Wang, Q.H. Recycling lower continental crust in the North China craton. *Nature* **2004**, *432*, 892–897. [CrossRef]
113. Green, H.T. Anatexis of mafic crust and high pressure crystallization of andesite. In *Andesites: Orogenic Andesites and Related Rocks*; Thorpe, R.S., Ed.; Wiley: London, UK, 1982; pp. 465–487.
114. Wang, Y. Geochemical characteristics of Beijing Baicha A-type granite and its genesis and tectonic indication significance. *J. Acta Petrol. Sin.* **2009**, *25*, 13–24. (In Chinese with English abstract)
115. Xu, J.F.; Castillo, P.R.; Li, X.H.; Yu, X.Y.; Zhang, B.R.; Han, Y.W. MORB-type rocks from the Paleo-Tethyan Mian-Lueyang northern ophiolite in the Qinling Mountains, central China: Implications for the source of the low $^{206}Pb/^{204}Pb$ and high $^{143}Nd/^{144}Nd$ mantle component in the Indian Ocean. *Earth Planet. Sci. Lett.* **2002**, *198*, 323–337. [CrossRef]
116. Xu, Z.Q.; Li, Y.; Liang, F.H.; Pei, X.Z. The connection of the Paleo-Tethys Suture zone in the Qinling-Dabie-Sulu Orogenic Belt. *Acta Geol. Sin.* **2015**, *89*, 671–680. (In Chinese with English abstract)
117. Hacker, B.R.; Ratschbacher, L.; Webb, L.E.; Ireland, T.R.; Walker, D.; Shuwen, D. U/Pb zircon ages constrain the architecture of the ultrahigh-pressure Qinling–Dabie Orogen, China. *Earth Planet. Sci. Lett.* **1998**, *161*, 215–230. [CrossRef]
118. Zhang, H.F.; Zhong, Z.Q.; Gao, S.; Zhang, B.R.; Li, H.M. Zircon U-Pb ages of the foliated eclogite granites in the west Dabie. *Chin. Sci. Bull.* **2001**, *46*, 843–846.
119. Qin, J.F.; Lai, S.C.; Li, Y.F. Slab Breakoff Model for the Triassic Post-Collisional Adakitic Granitoids in the Qinling Orogen, Central China: Zircon U-Pb Ages, Geochemistry, and Sr-Nd-Pb Isotopic Constraints. *Int. Geol. Rev.* **2008**, *50*, 1080–1104. [CrossRef]
120. Zhang, C.L.; Wang, T.; Wang, X.X. Origin and tectonic setting of the Early Mesozoic granitoids in Qinling Orogenic Belt. *Geol. China* **2008**, *14*, 304–316. (In Chinese with English abstract)
121. Zheng, Y.F.; Ye, K.; Zhang, L.F. Developing the plate tectonics from oceanic subduction to continental collision. *Chin. Sci. Bull.* **2009**, *54*, 2549–2555. [CrossRef]
122. Yin, Y.; Yin, X.M. Porphyry Cu-Mo-Au mineralization associated with Adakite and Himalayan granite in the northern margin of West Qinling. *Acta Petrol. Sin.* **2009**, *25*, 1239–1252. (In Chinese with English abstract)
123. Xu, X.Y.; Chen, J.L.; Gao, T.; Li, P.; Li, T. Granitic magmatism and tectonic setting in the northern margin of West Qinling. *Acta Petrol. Sin.* **2014**, *30*, 371–389. (In Chinese with English abstract)
124. Zhao, J.; Dong, Y.P.; Huang, B.C. Paleomagnetic Constraints of the Lower Triassic Strata in South Qinling Belt: Evidence for a Discrete Terrane between the North and South China Blocks. *Tectonics* **2020**, *39*, e2019TC005698. [CrossRef]
125. Rudnick, R.L. Making continental crust. *Nature* **1995**, *378*, 571–578. [CrossRef]
126. Zhang, Q.; Pan, G.Q.; Li, C.D.; Jin, W.J.; Jia, X.Q. Tectonic environment problems of granite: Reflections on granite research III. *Acta Petrol. Sin.* **2007**, *23*, 2683–2698.
127. Wang, T.; Wang, X.X.; Guo, L.; Zhang, L.; Tong, Y.; Li, S.; Huang, H.; Zhang, J.J. Granites and geotectonics. *Acta Petrol. Sin.* **2017**, *33*, 1459–1478.